

TTSnap: Test-Time Scaling of Diffusion Models via Noise-Aware Pruning

Qingtao Yu^α Changlin Song^α Minghao Sun^{α*} Zhengyang Yu^α Vinay Kumar Verma^β
 Soumya Roy^β Sumit Negi^β Hongdong Li^{α,β} Dylan Campbell^α
^α Australian National University ^β Amazon Research

{terry.yu, changlin.song, minghao.sun, zhengyang.yu, hongdong.li, dylan.campbell}@anu.edu.au

{vkvermaa, rosoumya, suminegi, hongdli}@amazon.com

Abstract

A prominent approach to test-time scaling for text-to-image diffusion models formulates the problem as a search over multiple noise seeds, selecting the one that maximizes a certain image-reward function. The effectiveness of this strategy heavily depends on the number and diversity of noise seeds explored. However, verifying each candidate is computationally expensive, because each must be fully denoised before a reward can be computed. This severely limits the number of samples that can be explored under a fixed budget. We propose test-time scaling with noise-aware pruning (TTSnap), a framework that prunes low-quality candidates without fully denoising them. The key challenge is that reward models are learned in the clean image domain, and the ranking of rewards predicted for intermediate estimates are often inconsistent with those predicted for clean images. To overcome this, we train noise-aware reward models via self-distillation to align the reward for intermediate estimates with that of the final clean images. To stabilize learning across different noise levels, we adopt a curriculum training strategy that progressively shifts the data domain from clean images to noise images. In addition, we introduce a new metric that measures reward alignment and computational budget utilization. Experiments demonstrate that our approach improves performance by over 16% compared with existing methods, enabling more efficient and effective test-time scaling. It also provides orthogonal gains when combined with post-training techniques and local test-time optimization. Code: <https://github.com/TerrysLearning/TTSnap/>.

1. Introduction

The success of recent large generative models is closely tied to scaling model capacities and data size during training [1, 4, 13, 21, 55, 63, 64]. However, an orthogonal direction for improving model performance has gained increas-

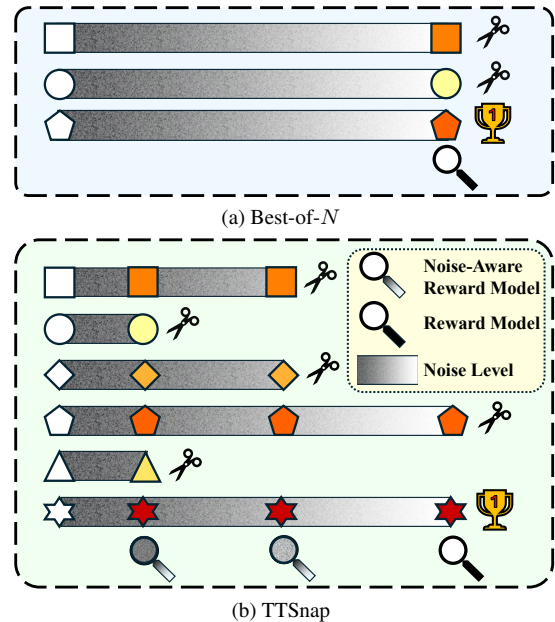


Figure 1. Comparison of the best-of- N TTS algorithm with our TTSnap algorithm under an equivalent compute budget. By applying early-stage pruning, TTSnap can explore a much larger pool of candidates (shown as polygons). Candidate colors indicate reward values from low (light yellow) to high (dark red). Each candidate is denoised from left to right under different initial noise. The magnifying glass represents the reward models, where the noise-aware variants are finetuned using our self-distillation strategy.

ing attention: scaling at test time [9, 30, 42, 47]. Test-time scaling (TTS) seeks to improve model performance by allocating additional compute during inference, instead of modifying the pretrained models themselves. While TTS has been widely explored for large language models with techniques like iterative reasoning [34, 59, 62] or multiple sampling passes [8, 54, 58], recent work has begun to extend this paradigm to diffusion and flow-matching models [10, 40, 56, 67].

Diffusion models generate samples by iteratively refin-

ing random noise towards the data distribution. Due to their inherent stochasticity, each generation process yields different outcomes, making search-based TTS design a natural and effective choice. Therefore, the core idea of TTS for diffusion models is to search a pool of candidate generations and select the one that maximizes a reward function. Despite the variety of proposed TTS frameworks [32, 33, 49, 53], the core principle remains consistent: under a given computational budget, search as many candidates as possible in the most promising regions of the search space.

All else being equal, searching over a larger and more diverse set of candidates increases the likelihood of obtaining high-quality results. For diffusion models, the primary source of stochasticity arises from the choice of initial noise [2, 14, 16, 78], making the initial noise space a prominent search dimension. However, this exploration is severely bottlenecked by its expensive computation: each candidate must be fully denoised before its quality can be verified, which restricts the number of candidates that can be explored under a fixed budget. To overcome this limitation, we propose to prune unpromising candidates early, using estimates obtained at earlier denoising stages rather than at the end of the process. To do so, we propose test time scaling with noise-aware pruning (TTSnap) to improve the efficiency of TTS for text-to-image diffusion models. An illustration of the pruning paradigm is shown in Fig. 1.

While early-stage pruning improves test-time efficiency, it introduces another challenge: inaccurate reward verification on intermediate estimates. Although more candidates can be explored, the risk of mistakenly pruning desirable ones increases because reward functions often assign rankings that are inconsistent with those obtained from fully denoised images. This mismatch arises because intermediate estimates are noisy and contain only coarse structural information, rather than high-frequency detail. Under such a noisy signal, reward models trained on the clean image domain fail to provide reliable scores.

To mitigate this issue, we make reward models noise-aware through a lightweight self-distillation process, allowing them to approximate the reward that a sample would have received once fully denoised. We obtain training data by sampling from a flow-based generative model starting from different Gaussian noise samples. For each trajectory, we compute intermediate estimates across all inference timesteps using posterior-mean reconstructions (Tweedie or Euler estimates) and store them as training samples. The training target for every intermediate estimate is the reward assigned to the final fully denoised image by a pretrained reward model, and the intermediate predictions are encouraged to match this final reward. Such a design brings two main advantages. First, it captures the marginal distribution of intermediate states of the diffusion process, ensuring that the training domain naturally aligns with the inference-time

distribution. Second, it requires no additional image data curation as all training samples are automatically generated. As a result, the training can be easily scaled.

To further enhance training effectiveness, we introduce two strategies: data diversity amplification and timestep curriculum learning. To increase training sample diversity and expose the model to a broader reward range, we apply the NegToMe [52] strategy to push individual trajectories farther apart and reduce image feature duplication. Moreover, the domain gap between clean images and intermediate images at timestep t increases as the level of noise increases (equivalently, t decreases). To obtain an effective noise-aware reward model with minimal pretraining effort, we adopt a curriculum strategy that gradually shifts learning from clean images to increasingly noisy ones, enabling smoother optimization. Since adjacent timesteps exhibit similar distributions, each timestep requires only a single training epoch. Compared with finetuning the entire diffusion model for reward alignment, our noise-aware reward self-distillation is far cheaper and more flexible, enabling high-quality image generation with a smaller additional effort to scale up test-time computation. Overall, our contributions are

1. an efficient noise-aware reward self-distillation strategy for extending reward models to the domain of noisy images; and
2. a test-time scaling strategy that uses this noise-aware reward model to optimally filter out low-promising candidates early to improve global search; and
3. three further takeaways:
 - (a) Generation *diversity* is critical for effective test-time scaling;
 - (b) Global search is *orthogonal* to post-training and test-time local optimization, and can be combined with them for further gains;
 - (c) We define a *metric* that jointly accounts for both budget and relative reward improvement to evaluate the performance of test-time scaling.

2. Related Work

Test-time Scaling. Test-time scaling aims to improve the performance of pre-trained models by allocating extra computation during inference [73]. For large language models, a common strategy is to enhance the reasoning process [18, 43]. Chain-of-thought prompting [34, 59, 62] generates intermediate reasoning steps to guide the final answer. Subsequent works refined this by iteratively correcting outputs [41, 42] or decomposing complex questions into simpler, sequential sub-problems [76]. Another approach samples multiple candidate solutions in parallel and selects the optimal one (*i.e.*, best-of- N) [8, 30, 54]. Test-time scaling also extends to vision-language models. EfficientTTS [23] performs inference-time adaptation by

jointly optimizing image and text prompts. VisVM [60] samples multiple reasoning paths and selects the best via a reward model. Recently, test-time scaling has been applied to diffusion models [10, 37, 40], including searching over initial noise [40, 67], exploring noise trajectories [33, 49], maximizing probability density along the denoising path [53, 56], and iteratively refining the conditional input [26, 32, 79]. Searching over the space of initial noise provides global benefits but incurs a high computational cost. In contrast, we focus on improving TTS efficiency in this setting through early-stage pruning.

Preference Alignment in Diffusion Models. The goal of preference alignment is to guide diffusion models toward outputs that better satisfy task objectives and align with human preferences. Post-training approaches typically leverage reward models via reinforcement learning [6, 11, 29, 51, 69, 75] or directly optimize diffusion models with human feedback [57, 66, 72]. For example, GRPO-based methods [38, 71] employ efficient gradient regularization to balance GPU memory usage and training stability while improving alignment quality. DPO-style methods further enhance preference alignment through step-aware preference modeling [35, 74]. Alternatively, some techniques achieve preference alignment during inference, without modifying the diffusion models. Some methods perform test-time optimization by refining the initial noise distribution [2, 14, 15, 77], while others intervene directly in the denoising trajectory [27, 68]. Meanwhile, the inherent stochasticity of diffusion models enables search-based strategies. In this paper, we investigate how to align rewards for diffusion models at test time within this search paradigm.

3. Preliminaries

In this section, we outline the technical background for image generation and test time scaling.

Forward and Reverse Diffusion Processes. We use the EDM [22] parameterization, commonly used in flow matching. In the diffusion forward process, the conditional distribution of the latent at timestep $t \in [0, 1]$ is formulated as

$$p(x_t|x_0) = \mathcal{N}(x_0, \sigma(t)^2 I), \quad (1)$$

where $x_0 \sim p_{\text{data}}$ and $\sigma(t)$ is the noise schedule. The sampling process integrates the trajectory from the prior noise distribution back to the target data distribution. This process is governed by the score function $\nabla_x \log p(x_t, \sigma(t))$, which is estimated by a neural network. The two primary forms defining this reverse process are

$$\text{ODE: } dx_t = -\dot{\sigma}(t)\sigma(t)\nabla_x \log p(x_t, \sigma(t))dt, \quad (2)$$

$$\text{SDE: } dx_t = -\dot{\sigma}(t)\sigma(t)\nabla_x \log p(x_t, \sigma(t))dt - \beta(t)\sigma(t)^2\nabla_x \log p(x_t, \sigma(t))dt + \sqrt{2\beta(t)}\sigma(t)dW_t, \quad (3)$$

where the ODE describes a deterministic trajectory, and the SDE defines a stochastic sampling path via the Wiener process W_t and a compensating deterministic decay term β , preserving the same marginal distribution of x_t [22].

Posterior Mean Approximation. During intermediate sampling, when only x_t is observable, the expected clean data $\hat{x}_0(t) = \mathbb{E}[x_0 | x_t]$ can be estimated via Tweedie’s formula [12, 50], given by

$$\hat{x}_0(t) = x_t + \sigma(t)^2\nabla_x \log p(x_t, \sigma(t)). \quad (4)$$

In practice, $\hat{x}_0(t)$ represents a blurred approximation of x_0 that retains mainly high-level structure when t is large. As t decreases, finer details are progressively restored, converging to the fully denoised clean data.

Test Time Scaling for Diffusion Models. The inference cost of T2I diffusion models can be naturally scaled by increasing the number of denoising steps, but this yields rapidly diminishing returns [40]. A more effective strategy is to search over a pool of sampled candidates to identify the one that leads to the highest quality generation [33, 40, 49, 53, 67]. This process relies on diverse samples and two key components: a verifier and a search algorithm. Verifiers are typically pretrained lightweight reward models [28, 48, 65, 69] that evaluate the quality of generated image candidates. Conditioned on an input text prompt $p \in \mathcal{P}$, the verifier is formulated as

$$\psi : \mathbb{R}^{H \times W \times C} \times \mathcal{P} \rightarrow \mathbb{R}, \quad (5)$$

and may not be differentiable with respect to the inference trajectory. The search algorithm aims to identify the most promising candidates that maximize the verifier’s reward scores. The algorithm f takes the verifier $\psi \in \Psi$, the diffusion model $\phi \in \Phi$, and N candidate image samples with text conditions as input and returns an image:

$$f : \Psi \times \Phi \times \mathbb{R}^{N \times H \times W \times C} \times \mathcal{P}^N \rightarrow \mathbb{R}^{H \times W \times C}. \quad (6)$$

Increasing the number of candidates N increases the probability of finding a high-reward sample, but also increases the inference-time compute cost. Among various search algorithms, best-of- N is the most straightforward yet effective one [40, 67]. This algorithm independently samples N Gaussian noise, denoises each, and verifies their rewards. Its core advantage lies in enabling global exploration across the initial noise space. Other strategies, such as greedy neighborhood search [40, 49] or trajectory-level search [17, 25, 33, 40, 53], primarily focus on finding locally optimal candidates. In this paper, we mainly focus on improving TTS over best-of- N , since a more global search, as discussed in Sec. 6.3, typically yields better performance. While some methods scale performance by refining the conditioning signals [26, 32, 79], we focus our study to the setting where the text condition remains fixed.

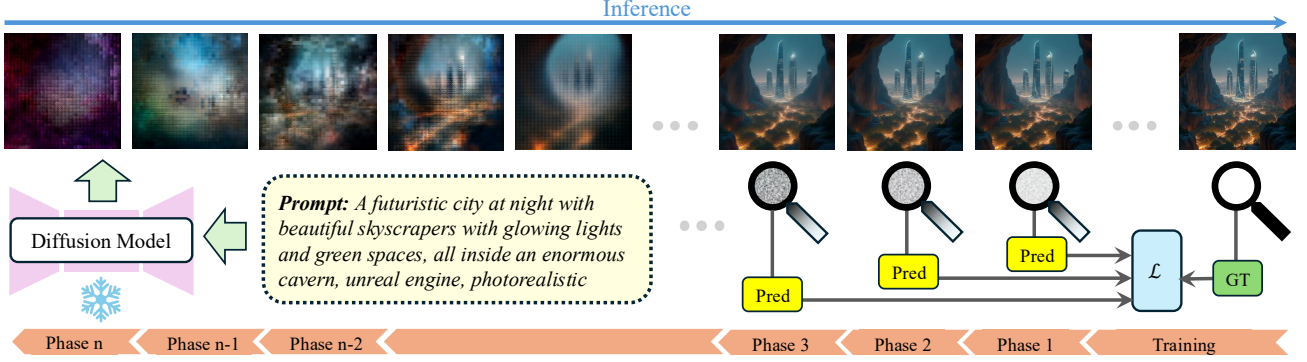


Figure 2. Noise-aware reward finetuning. Given a set of text prompts, we generate training data by sampling from the diffusion model and storing the intermediate Tweedie-estimated images. To train the noise-aware reward models, we introduce a curriculum self-distillation strategy that gradually shifts the training domain from clean images to increasingly noisy ones. After one epoch at each noise level, we save the model weights and proceed to the next, ensuring small domain gaps and stable, efficient training.

4. The TTSnap Algorithm

The primary limitation of the best-of- N strategy lies in its high verification cost, as each candidate must be fully denoised before reward evaluation. This constraint severely restricts the breadth of candidate exploration under a fixed computational budget. To address this inefficiency, we propose a pruning strategy, outlined in Algorithm 1, that verifies and eliminates unpromising candidates early in the denoising process. Since the reward models operate in the image domain, we approximate the image corresponding to an intermediate latent by estimating its posterior mean, detailed in Sec. 3, and decoding it via the variational auto-encoder (VAE) decoder. The intermediate images are then scored by the reward model, and candidates with low rewards are pruned according to a predefined retention ratio. This process is iterated until the final step, where the remaining candidates are fully denoised, and the one yielding the highest reward is selected as the output. The set of verification timesteps is denoted as $\mathcal{T} = \{\tau_1, \dots, \tau_{m-1}\} \subseteq [1, M-1]$, where $\tau_{m-1} = M-1$. M is the final timestep. The set of corresponding retention ratios is $\mathcal{A} = \{\alpha_1, \dots, \alpha_{m-1}\}$, where $0 < \alpha_i < 1$ is the fraction of candidates that will be retained at timestep τ_i .

Budget Analysis. By avoiding the full denoising of every candidate, such an algorithm can substantially reduce the overall compute cost. However, it introduces additional verification overhead: VAE decoding and reward computation. Let the computational cost of a single denoising step for one candidate be B_d , and that of a single verification be B_v . For N initial candidates, the total compute budget B can be expressed as

$$B = \sum_{i=1}^m \prod_{j=0}^{i-1} \alpha_j ((\tau_i - \tau_{i-1})B_d + B_v) N, \quad (7)$$

Algorithm 1: TTSnap

Input: verification timesteps \mathcal{T} ; retention ratios \mathcal{A} ; number of initial candidates N ; number of diffusion inference steps M ; diffusion denoising operation ϕ ; VAE decoder ν ; reward model ψ ; text prompt p

Output: image \mathcal{I}

```

1  $\mathcal{X} \leftarrow \{x^i \mid x^i \sim \mathcal{N}(0, I), i \in [1, N]\}$ 
2 for  $j = 1$  to  $M$  do
3    $\mathcal{X}' \leftarrow \{x' \mid x' = \phi(x, p), x \in \mathcal{X}\}$ 
4   if  $j = M$  then
5      $\mathcal{R} \leftarrow \{r \mid r = \psi(\nu(x), j), x \in \mathcal{X}'\}$ 
6      $i \leftarrow \arg \max(\mathcal{R})$ 
7      $\mathcal{I} \leftarrow \nu(\mathcal{X}_i)$ 
8     return  $\mathcal{I}$ 
9   else if  $j \in \mathcal{T}$  then
10     $\mathcal{R} \leftarrow \{r \mid r = \psi(\nu(x), j), x \in \mathcal{X}'\}$ 
11     $k \leftarrow \mathcal{A}_{\text{index}(j, \mathcal{T})} |\mathcal{R}|$ 
12     $\mathcal{X} \leftarrow \{\mathcal{X}_i \mid i \in \arg \text{topk}(\mathcal{R}, k)\}$ 

```

where $\tau_0 := 0$ and $\alpha_0 := 1$. Thus for a fixed budget B , the number of candidates that can be explored is

$$N = \left\lfloor \frac{B}{\sum_{i=1}^m \prod_{j=0}^{i-1} \alpha_j ((\tau_i - \tau_{i-1})B_d + B_v)} \right\rfloor. \quad (8)$$

Under the same compute budget B , our N is much larger than that of the original best-of- N strategy: $N = \lfloor B / (MB_d + B_v) \rfloor$.

Performance Evaluation. The primary goal of TTS is to maximize the generated image quality with minimal computational cost. Existing TTS methods are typically evaluated under a fixed computation budget or by visualizing the relationship between the final reward and compu-

tational cost [32, 33, 40]. Such evaluations are often indirect. Hence, we introduce a new metric that quantifies performance improvement as the computation budget increases. Let $f(N)$ denote the final image obtained from algorithm f with N noise candidates, as described in Eq. (6), and let $\psi(f(N))$ represent its corresponding reward score. The number of explored candidates N can be determined from a given computation budget B , such as Eq. (8) for our method. Over a budget range $[B^-, B^+]$, we define the incremental performance gain with respect to budget B as

$$g_f(B) = \psi(f(N(B))) - \psi(f(N(B^-))). \quad (9)$$

To measure overall efficiency, we integrate the gain over the budget interval

$$h_f = \int_{B^-}^{B^+} g_f(B) dB. \quad (10)$$

To compare the target algorithm f_{tar} with a reference algorithm f_{ref} , the relative performance ω is formulated as

$$\omega(f_{\text{tar}}, f_{\text{ref}}) = \frac{h_{f_{\text{tar}}} - h_{f_{\text{ref}}}}{h_{f_{\text{ref}}}}. \quad (11)$$

This metric evaluates the relative improvement in reward growth as a function of compute, independent of the absolute reward scale.

5. Noise-Aware Reward Finetuning (NARF)

While the proposed TTSnap algorithm improves the exploration bandwidth of test-time scaling, its performance does not further increase when directly applying clean-image reward models to intermediate denoising steps. This limitation arises from the large domain gap between the reward model training data (clean images) and the test data in this setting (Tweedie estimates). Images decoded at earlier timesteps do not contain as much high-frequency detail as those decoded near the end of denoising, which leads to inconsistent reward ranking. To address this issue, we finetune the reward model using a self-distillation strategy to better adapt to the early-timestep image domain.

Self-distillation. We leverage a self-distillation strategy to align a noise-aware reward model with the final clean-image rewards. Training samples are obtained by running the diffusion model with random initial noise and recording the intermediate decoded images using Tweedie estimates. For each trajectory, the reward computed on the final clean image is used as the supervisory signal, and the rewards predicted for all intermediate images are trained to match this target. The loss is the mean squared error between the predicted reward for the intermediate image and the predicted reward for the clean image. This approach allows the noise-aware reward model to capture the true marginal distribution encountered during inference. It is also highly scalable:

it only requires the diffusion model and a set of prompts—no additional data.

Enhancing Data Diversity. Reward models trained on clean-image domains typically rely on human-annotated positive—negative image pairs that exhibit clear quality differences [28, 65, 69]. In contrast, images generated with the same prompt in our pipeline may appear similar and have similar reward scores, despite starting from different initial noise. This redundancy reduces the effectiveness of training. To increase the diversity of the training data, we use the strategy from NegToMe [52], which pushes individual generative trajectories farther apart by reducing the influence of duplicated features within a batch.

Curriculum Training. Finetuning a reward model at noisier timesteps is more difficult than at cleaner timesteps, since the domain gap is greater. To alleviate this, we adopt an easy-to-hard training data curriculum: starting with near-clean images and incrementally increasing the data noise level, saving the model parameters for each timestep. Since the domain gap between adjacent timesteps is small, we find that a single training epoch per timestep is sufficient. This is an efficient strategy for training a set of noise-aware reward models and also helps the model converge to better optima. The training process is illustrated in Fig. 2.

6. Experiments

First, we validate the effectiveness of our proposed noise-aware training design (NARF) across different reward models. Then, we evaluate and analyze the performance of our TTSnap framework equipped with these fine-tuned noise-aware reward models. We use Flux-1.dev [3] as the diffusion model with 20 inference steps and a guidance scale of 3.5. For NegToMe [52], we set the merging alpha to 1.2 and the merging threshold to 0.65. We use ImageReward [69], HPS[65], and PickScore[28] as reward models, all of which measure text-to-image alignment, aesthetics, and subjective human preference. All prompts used in this section are sourced from the ImageReward dataset [69]. We also evaluate our approach on SDXL [46] to test the generalization of both NARF and TTSnap in Appendix Sec. A.

6.1. NARF Experiments

Training Details. For the training dataset, we generate 8 samples per prompt across 5000 prompts, with each sample coming with 20 intermediate decoded images corresponding to all the inference stages. The training starts from the 15th to the 1st timestep. Each timestep is trained for one epoch and the resulting checkpoint is used as the initialization for the subsequent timestep. The batch sizes for ImageReward, HPS and PickScore are set as 100, 50 and 50; while learning rates are set as 3e-6, 5e-6 and 5e-7 with a lin-

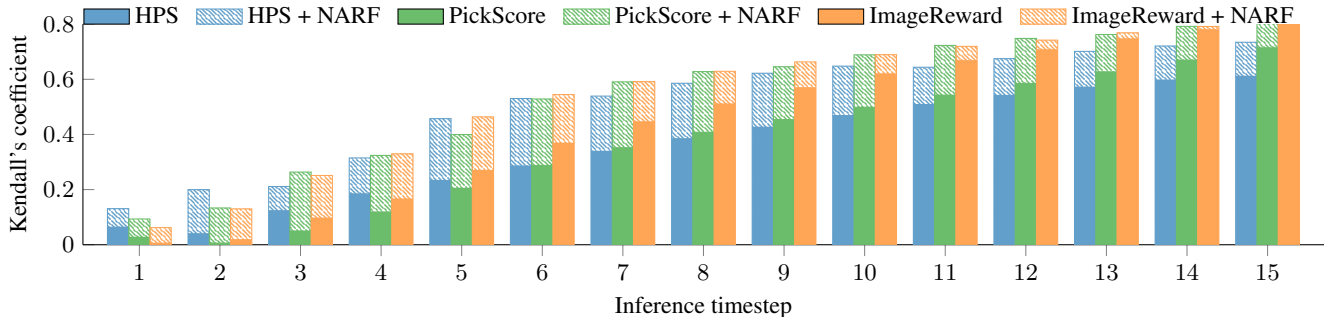


Figure 3. Rank consistency at different noise levels (noisier timesteps to the left), for three reward models, with and without our noise-aware reward finetuning (NARF) approach.

ear scheduler. Training each reward model takes two hours on $4 \times A100$ GPUs.

Results. We construct a validation set using 200 prompts unseen during training, generating 80 samples per prompt along with all corresponding intermediate images. For the purpose of TTS, our goal is to ensure that reward predictions at early inference stages preserve a ranking similar to the final clean-image counterparts. To measure this rank consistency, we compute Kendall’s τ coefficient [24] between the noise-aware reward scores at early timesteps and the final-step reward scores for each prompt, and report the average correlation across all prompts on the validation set. Kendall’s τ measures the ordinal agreement between two ranked lists, taking values from 1 (identical order) to -1 (complete reversal). It reflects the normalized number of pairwise swaps needed to turn one ranking into the other, independent of the value magnitudes. As shown in Fig. 3, our noise-aware reward self-distillation consistently improves early-stage ranking agreement across all three reward models compared with their un-finetuned baselines. This substantial gain in rank consistency makes our early-step pruning framework more reliable and effective. A further analysis of NARF and a comparison with its alternatives are presented in Appendix Sec. B.

6.2. TTSnap Experiments

Experiment Setup. We take the fine-tuned noise-aware reward model from the previous section and evaluate our TTSnap algorithm on the validation prompts. The computation budget is measured in TFLOPs. We cap the maximum budget at 4,000 TFLOPs, which approximately equals 400 forward passes of the Flux diffusion transformer. Our main evaluation metric is w as defined in Eq. (11), representing the increase ratio of the integral of reward improvement over budget, with reference to the best-of- N baseline. To mitigate randomness and ensure a fair comparison across different TTSnap configurations, we generate a pool of over 200 candidate trajectories for each prompt and constrain all search procedures to operate within this shared pool. For

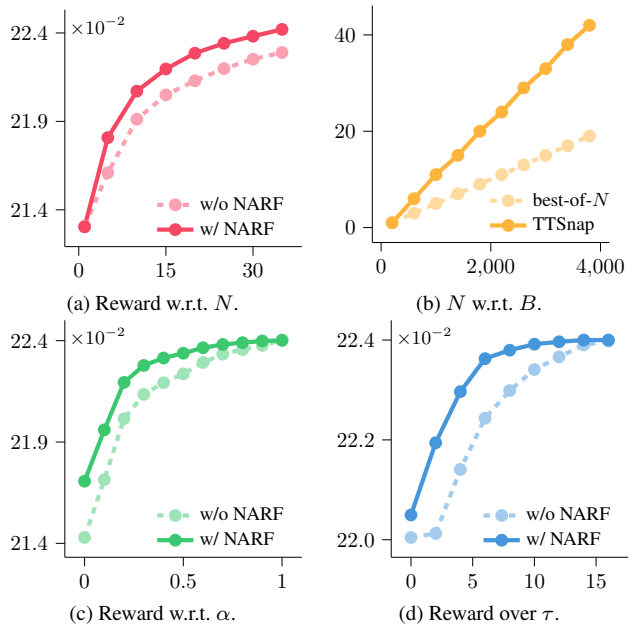


Figure 4. Analysis of the effect of different variables on the PickScore reward or number of explored samples N , with respect to (a) N , (b) the compute budget B , (c) the retention ratio α , and (d) the pruning timestep τ , and compare with the baselines. Defaults of N , B , α , τ are 35, 4000, 0.3 and 6.

each search, we iterate 100 times over different seeds and report the average reward of the final selected image.

Variable Analysis. To illustrate how the TTSnap parameters contribute to the reward of the final selected image, we provide a one-stage pruning analysis in Fig. 5 with PickScore. From Fig. 4a, increasing the number of candidates (N) consistently improves the final rewards, and our finetuned noise-aware reward model converges faster as N grows compared to baseline models, since it provides more accurate intermediate reward estimates. Fig. 4b highlights another key reason why TTSnap outperforms best-of- N . With pruning, we can explore many more candidates un-

Table 1. Optimal search parameters for multi-stage pruning with our noise-aware PickScore reward model. We report the relative performance improvement across a range of budgets ω , with respect to the best-of- N strategy.

$ \mathcal{T} $	best \mathcal{T}	best \mathcal{A}	ω
1	{6}	{0.3}	13.82%
2	{3, 7}	{0.4, 0.3}	16.07%
3	{3, 7, 12}	{0.4, 0.4, 0.5}	17.41%
4	{3, 6, 9, 12}	{0.5, 0.5, 0.8, 0.8}	16.67%
5	{3, 6, 8, 10, 13}	{0.6, 0.6, 0.8, 0.8, 0.8}	16.26%

der the same compute budget. In Fig. 4c and Fig. 4d, we examine the effect of the retention ratio α and the pruning timestep τ . A larger α and a later pruning stage τ both lead to better results, since they reduce the risk of discarding promising trajectories. As indicated by our cost formulation in Eq. (7), increasing α or τ raises the computational cost linearly, while the performance improves quickly at first but then gradually flattens out, resulting in diminishing marginal gains.

Multi-Stage Pruning. TTSnap performance can be further improved by extending the algorithm to a multi-stage pruning setup. We search for the optimal parameter settings across different numbers of pruning stages, as shown in Tab. 1, and performance is evaluated using Eq. (11) within our budget range. According to Eq. (7) and Eq. (8), adding more stages saves budget and allows a broader exploration of candidates, but it also accumulates more reward estimation errors. As a result, when using more stages, the retention ratios α should be set slightly higher, especially in later timesteps when fewer candidates remain. While increasing a certain number of pruning stages improves performance, too many stages become counterproductive, since the verification cost would be highly increased, eventually reducing performance under budget forcing. For comparison, we also search for the best parameter settings for rewards without noise-aware finetuning (NARF) and plot them with the best-of- N baseline in Fig. 5a. As shown in the figure, while best-of- N requires 4000 TFLOPs to reach that reward level, our method achieves it with only 2400 TFLOPs.

Multi-Reward Verification. We search for general optimal hyperparameter settings that yield the best average performance across all reward models. Specifically, we set the verification timesteps \mathcal{T} to [5, 7, 12] and the retention ratios \mathcal{A} to [0.4, 0.5, 0.6]. For comparison, we apply the same hyperparameter search procedure to the baseline reward without NARF, where the best settings are $\mathcal{T} = [7, 13]$ and $\mathcal{A} = [0.6, 0.7]$. As shown in Tab. 2, our method achieves multifold improvements over the baseline in terms of ω from Eq. (11) and the output reward across different compute budgets. We further extend TTSnap to include

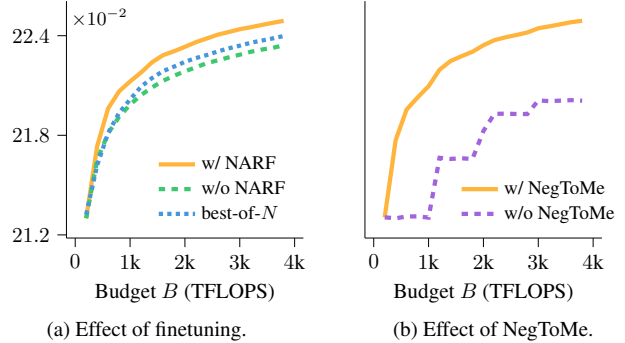


Figure 5. The PickScore reward of the final image with respect to the budget B for (a) TTSnap (w/ NARF), TTSp (w/o NARF), and best-of- N , and (b) TTSnap with and without NegToMe sample diversity enhancement.

Table 2. Comparison of the best-of- N (BoN) strategy, pruning without NARF (TTSp), and pruning with NARF (TTSnap) under single-reward and combined-reward settings. The top row indicates the reward model used by the algorithm and the second row indicates the reward model used for evaluation. We report the final reward values for compute budgets $B = 1k, 2k, 4k$ TFLOPs, along with the relative gain ω over best-of- N . $r(B \rightarrow 0)$ denotes the expected reward of sampling one image per prompt at random.

	Alg. Reward:	IR	Pick	HPS	All	All	All
	Eval. Reward:	IR	Pick	HPS	IR	Pick	HPS
-	$r(B \rightarrow 0)$.905	.2139	.2803	.843	.2129	.2791
BoN	$r(B = 1k)$	1.315	.2198	.2883	1.185	.2184	.2862
	$r(B = 2k)$	1.427	.2219	.2911	1.280	.2198	.2883
	$r(B = 4k)$	1.501	.2234	.2934	1.348	.2210	.2899
TTSp	$r(B = 1k)$	1.348	.2208	.2886	1.206	.2185	.2869
	$r(B = 2k)$	1.454	.2223	.2915	1.295	.2201	.2889
	$r(B = 4k)$	1.525	.2238	.2939	1.360	.2213	.2906
	ω (%)	3.3	2.4	1.8	2.4	0.7	5.1
TTSnap	$r(B = 1k)$	1.386	.2212	.2891	1.228	.2193	.2874
	$r(B = 2k)$	1.504	.2232	.2930	1.313	.2212	.2902
	$r(B = 4k)$	1.566	.2248	.2952	1.375	.2223	.2919
	ω (%)	14.6	16.6	15.8	10.9	20.4	21.8

multiple reward models jointly within a single search process, aiming to find the best candidates across different evaluative aspects. Since different rewards may have varying scales, we record the relative rankings of each metric across samples and use the sum of these ranks as a combined reward for each candidate [40]. As shown in the last three columns in Tab. 2, under the joint-reward search paradigm, our method continues to achieve large gains across all three rewards compared with the baseline. Qualitative results are visualized in Fig. 6.

Adorable strawberry critter

					
IR: 1.511 Pick: 0.2297 HPS: 0.2819	IR: 0.171 Pick: 0.2189 HPS: 0.2560	IR: 1.720 Pick: 0.2337 HPS: 0.2789	IR: 1.787 Pick: 0.2347 HPS: 0.2830	IR: 1.833 Pick: 0.2385 HPS: 0.2863	IR: 1.872 Pick: 0.2401 HPS: 0.2900

The cursed vampire knight in the moonlight by Kev Walker and Noah Bradley and Delphin Enjolras and Daniel f. Gerhartz

					
IR: 0.604 Pick: 0.1819 HPS: 0.2251	IR: 0.919 Pick: 0.1986 HPS: 0.2498	IR: 0.614 Pick: 0.2006 HPS: 0.2520	IR: 1.113 Pick: 0.2059 HPS: 0.2584	IR: 1.469 Pick: 0.2021 HPS: 0.2561	IR: 1.651 Pick: 0.2061 HPS: 0.2617

A swimming pool at the bottom of the ocean

					
IR: 0.542 Pick: 0.2131 HPS: 0.2347	IR: 0.106 Pick: 0.2204 HPS: 0.2785	IR: -1.468 Pick: 0.2213 HPS: 0.2770	IR: 1.370 Pick: 0.2264 HPS: 0.2670	IR: 1.522 Pick: 0.2293 HPS: 0.3090	IR: 1.606 Pick: 0.2327 HPS: 0.3107
Random			Best-of-N	TTS_p	TTSnap (Ours)

Figure 6. Qualitative comparison of three one-pass generations from random noise, best-of- N search, pruning without NARF (TTS_p) and with NARF (TTSnap), under the multi-reward verification setting. The compute budget for the last three methods is set to 4000 TFlops.

6.3. Discussion

Diversity Matters. To evaluate the role of candidate diversity in our algorithm, we remove the NegToMe [52] strategy when creating the validation set and re-test TTSnap under the same hyperparameter settings, as shown in Fig. 5b. We observe that when diversity is reduced, the reward curve growth drops noticeably. This occurs for two reasons: diverse samples naturally exhibit higher reward variance, which improves ranking accuracy in the early stage. More importantly, higher diversity reduces the chance of generating similar samples, preventing redundant verifications.

Given the above observation, more global exploration generally leads to stronger TTS performance. Our method focuses on maximizing the number of explored candidates within a given budget. In contrast, some approaches con-

sider an orthogonal direction that prioritizes local refinement around promising candidates [33, 40, 49]. Their motivation is that global search over the initial noise samples, as used in best-of- N and our method, carries the risk of reward hacking [44]. However, this risk can be effectively controlled by limiting the search size N or by using multiple reward models to provide verification signals from different perspectives. As demonstrated in Tab. 2, reducing N or combining multiple rewards helps prevent the output images from overfitting to any single reward model.

Compatibility While TTSnap enhances test-time global search of diffusion models, it is also orthogonal to post-training and local test-time optimization methods. TTSnap can be seamlessly integrated with them and used as a plug-in to further boost their inference performance. We vali-

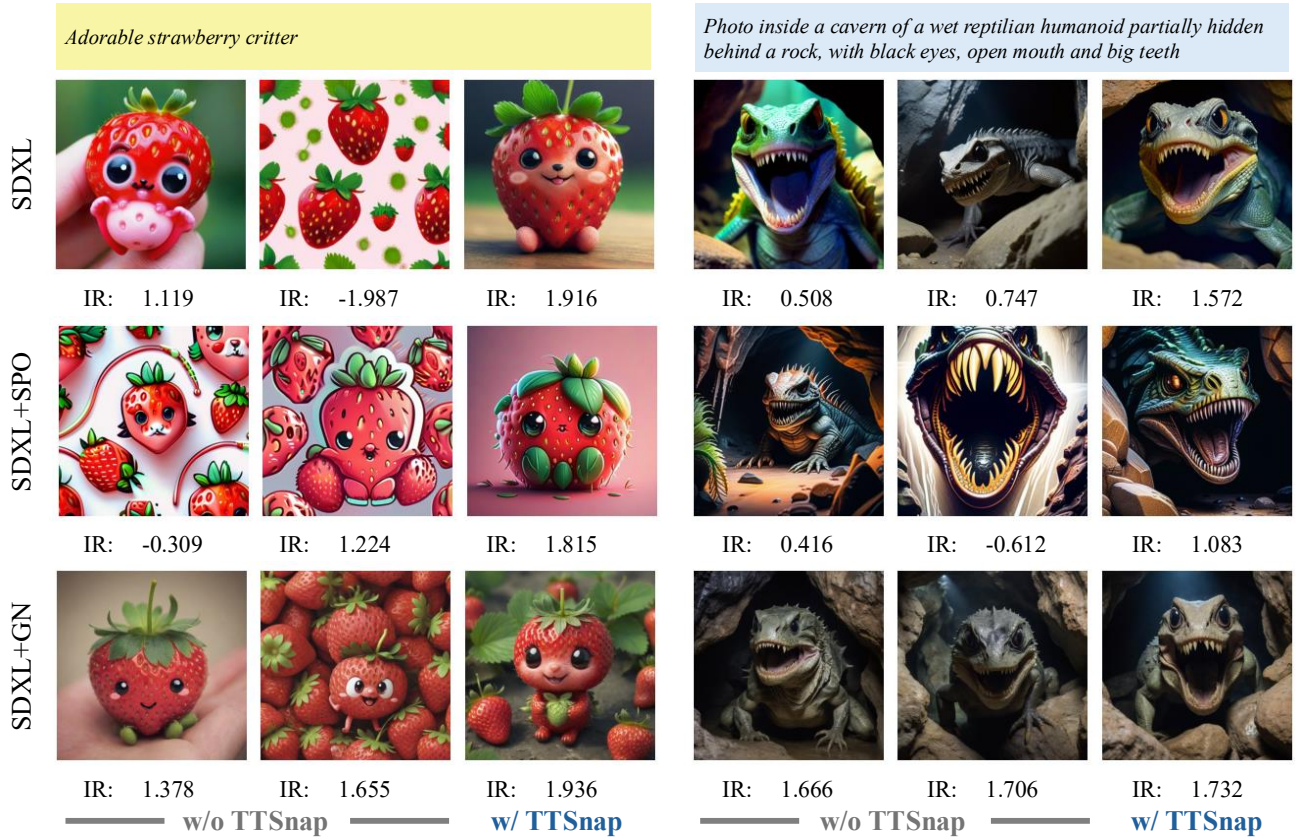


Figure 7. Qualitative comparisons of applying TTSnap on SDXL, SDXL + SPO post-training, and SDXL + Golden Noise local optimization. Our TTSnap global search operates as a plug-in and can be combined with any of these methods to further improve output quality. For each prompt, the left two columns show the results without TTSnap, while the right column shows the results after applying TTSnap.

date this compatibility through experiments on SDXL [46]. For example, SPO [35] finetunes SDXL to align with PickScore, leading to enhanced aesthetic quality. We apply TTSnap with ImageReward on this finetuned model, offering a complementary enhancement with a different reward model. shift the model’s distribution bias to pickscore, For local optimization, we incorporate Golden Noise [77] to refine each initial noise and subsequently apply TTSnap with ImageReward to search for the best candidate. This combination enables us to discover higher-quality candidates than either method alone. Quantitative and qualitative comparisons are presented in Tab. 3 and Fig. 7.

7. Conclusion

We have presented an efficient test-time scaling strategy that employs pruning with noise-aware reward models, along with a self-distillation strategy for training them from a set of prompts. This greatly increases the number of image candidates to explore within a given compute budget, improving the expected quality of the final image. Our method improves performance across a range of budgets with sin-

Table 3. Quantitative results of applying TTSnap with ImageReward on SDXL, SDXL + SPO post-training, and SDXL + Golden Noise local optimization. We report the ImageReward scores of TTSnap under compute budgets of $B = 1k, 2k, 4k$.

	SDXL	SDXL + SPO	SDXL + GN
w/o TTSnap	0.821	0.585	1.196
TTSnap ($B = 1k$)	1.396	1.289	1.460
TTSnap ($B = 2k$)	1.470	1.391	1.510
TTSnap ($B = 4k$)	1.515	1.445	1.538

gle or combined reward models, and we highlight sample diversity as a crucial axis for test-time scaling.

Acknowledgments

We would like to thank Xingjian Leng and Zhanhao Liang for helpful discussions and feedback on experiment design. We are also deeply appreciative of Jaskirat Singh for his work on negative token merging.

References

- [1] Josh Achiam, Steven Adler, Sandhini Agarwal, Lama Ahmad, Ilge Akkaya, Florencia Leoni Aleman, Diogo Almeida, Janko Altenschmidt, Sam Altman, Shyamal Anadkat, et al. Gpt-4 technical report. *arXiv preprint arXiv:2303.08774*, 2023. 1
- [2] Donghoon Ahn, Jiwon Kang, Sanghyun Lee, Jaewon Min, Minjae Kim, Wooseok Jang, Hyoungwon Cho, Sayak Paul, SeonHwa Kim, Eunju Cha, et al. A noise is worth diffusion guidance. *arXiv preprint arXiv:2412.03895*, 2024. 2, 3
- [3] B. F. Labs. Flux.1 [dev]. Website. Accessed: November 8, 2025. 5, 1
- [4] Jinze Bai, Shuai Bai, Yunfei Chu, Zeyu Cui, Kai Dang, Xiaodong Deng, Yang Fan, Wenbin Ge, Yu Han, Fei Huang, et al. Qwen technical report. *arXiv preprint arXiv:2309.16609*, 2023. 1
- [5] Lital Binyamin, Yoad Tewel, Hilit Segev, Eran Hirsch, Royi Rassin, and Gal Chechik. Make it count: Text-to-image generation with an accurate number of objects. In *Proceedings of the Computer Vision and Pattern Recognition Conference*, pages 13242–13251, 2025. 3
- [6] Kevin Black, Michael Janner, Yilun Du, Ilya Kostrikov, and Sergey Levine. Training diffusion models with reinforcement learning. In *The Twelfth International Conference on Learning Representations*, 2024. 3
- [7] Ralph Allan Bradley and Milton E Terry. Rank analysis of incomplete block designs: I. the method of paired comparisons. *Biometrika*, 39(3/4):324–345, 1952. 1, 3
- [8] Bradley Brown, Jordan Juravsky, Ryan Ehrlich, Ronald Clark, Quoc V Le, Christopher Ré, and Azalia Mirhoseini. Large language monkeys: Scaling inference compute with repeated sampling. *arXiv preprint arXiv:2407.21787*, 2024. 1, 2
- [9] Zhe Chen, Weiyun Wang, Yue Cao, Yangzhou Liu, Zhangwei Gao, Erfei Cui, Jinguo Zhu, Shenglong Ye, Hao Tian, Zhaoyang Liu, et al. Expanding performance boundaries of open-source multimodal models with model, data, and test-time scaling. *arXiv preprint arXiv:2412.05271*, 2024. 1
- [10] Zhekai Chen, Ruihang Chu, Yukang Chen, Shiwei Zhang, Yujie Wei, Yingya Zhang, and Xihui Liu. Tts-var: A test-time scaling framework for visual auto-regressive generation. *arXiv preprint arXiv:2507.18537*, 2025. 1, 3
- [11] Kevin Clark, Paul Vicol, Kevin Swersky, and David J Fleet. Directly fine-tuning diffusion models on differentiable rewards. In *The Twelfth International Conference on Learning Representations*. 3
- [12] Bradley Efron. Tweedie’s formula and selection bias. *Journal of the American Statistical Association*, 106(496):1602–1614, 2011. 3
- [13] Patrick Esser, Sumith Kulal, Andreas Blattmann, Rahim Entezari, Jonas Müller, Harry Saini, Yam Levi, Dominik Lorenz, Axel Sauer, Frederic Boesel, et al. Scaling rectified flow transformers for high-resolution image synthesis. In *Forty-first international conference on machine learning*, 2024. 1
- [14] Luca Eyring, Shyamgopal Karthik, Karsten Roth, Alexey Dosovitskiy, and Zeynep Akata. Reno: Enhancing one-step text-to-image models through reward-based noise optimization. *Advances in Neural Information Processing Systems*, 37:125487–125519, 2024. 2, 3
- [15] Luca Eyring, Shyamgopal Karthik, Alexey Dosovitskiy, Nataniel Ruiz, and Zeynep Akata. Noise hypernetworks: Amortizing test-time compute in diffusion models. *arXiv preprint arXiv:2508.09968*, 2025. 3
- [16] Luca Eyring, Shyamgopal Karthik, Alexey Dosovitskiy, Nataniel Ruiz, and Zeynep Akata. Noise hypernetworks: Amortizing test-time compute in diffusion models. *arXiv preprint arXiv:2508.09968*, 2025. 2
- [17] Guilherme Fernandes, Vasco Ramos, Regev Cohen, Idan Szpektor, and Joao Magalhaes. Latent beam diffusion models for generating visual sequences. *arXiv preprint arXiv:2503.20429*, 2025. 3
- [18] Daya Guo, Dejian Yang, Haowei Zhang, Junxiao Song, Ruoyu Zhang, Runxin Xu, Qihao Zhu, Shirong Ma, Peiyi Wang, Xiao Bi, et al. Deepseek-r1: Incentivizing reasoning capability in llms via reinforcement learning. *arXiv preprint arXiv:2501.12948*, 2025. 2
- [19] Kaiyi Huang, Chengqi Duan, Kaiyue Sun, Enze Xie, Zhenguo Li, and Xihui Liu. T2i-combench++: An enhanced and comprehensive benchmark for compositional text-to-image generation. *IEEE Transactions on Pattern Analysis and Machine Intelligence*, 2025. 3
- [20] Zhiwei Jia, Yuesong Nan, Huixi Zhao, and Gengdai Liu. Reward fine-tuning two-step diffusion models via learning differentiable latent-space surrogate reward. In *Proceedings of the Computer Vision and Pattern Recognition Conference*, pages 12912–12922, 2025. 3
- [21] Jared Kaplan, Sam McCandlish, Tom Henighan, Tom B Brown, Benjamin Chess, Rewon Child, Scott Gray, Alec Radford, Jeffrey Wu, and Dario Amodei. Scaling laws for neural language models. *arXiv preprint arXiv:2001.08361*, 2020. 1
- [22] Tero Karras, Miika Aittala, Timo Aila, and Samuli Laine. Elucidating the design space of diffusion-based generative models. In *NeurIPS*, pages 26565–26577, 2022. 3
- [23] Mehmet Onurcan Kaya, Desmond Elliott, and Dim P. Papadopoulos. Efficient test-time scaling for small vision-language models. *arXiv preprint arXiv:2510.03574*, 2025. 2
- [24] M. G. KENDALL. A new measure of rank correlation. *Biometrika*, 30(1-2):81–93, 1938. 6, 3
- [25] Jaihoon Kim, Taehoon Yoon, Jisung Hwang, and Minhyuk Sung. Inference-time scaling for flow models via stochastic generation and rollover budget forcing. *arXiv preprint arXiv:2503.19385*, 2025. 3
- [26] Semin Kim, Yeonwoo Cha, Jaehoon Yoo, and Seunghoon Hong. Reward-agnostic prompt optimization for text-to-image diffusion models. *arXiv preprint arXiv:2506.16853*, 2025. 3
- [27] Sunwoo Kim, Minkyu Kim, and Dongmin Park. Test-time alignment of diffusion models without reward over-optimization. *arXiv preprint arXiv:2501.05803*, 2025. 3
- [28] Yuval Kirstain, Adam Polyak, Uriel Singer, Shahbuland Matiana, Joe Penna, and Omer Levy. Pick-a-pic: An open

- dataset of user preferences for text-to-image generation. In *NeurIPS*, pages 36652–36663, 2023. 3, 5
- [29] Kimin Lee, Hao Liu, Moonkyung Ryu, Olivia Watkins, Yuqing Du, Craig Boutilier, Pieter Abbeel, Mohammad Ghavamzadeh, and Shixiang Shane Gu. Aligning text-to-image models using human feedback. *arXiv preprint arXiv:2302.12192*, 2023. 3
- [30] Dacheng Li, Shiyi Cao, Chengkun Cao, Xiuyu Li, Shangyin Tan, Kurt Keutzer, Jiarong Xing, Joseph E Gonzalez, and Ion Stoica. S*: Test time scaling for code generation. *arXiv preprint arXiv:2502.14382*, 2025. 1, 2
- [31] Junnan Li, Dongxu Li, Caiming Xiong, and Steven Hoi. Blip: Bootstrapping language-image pre-training for unified vision-language understanding and generation. In *International conference on machine learning*, pages 12888–12900. PMLR, 2022. 3
- [32] Shufan Li, Konstantinos Kallidromitis, Akash Gokul, Arsh Koneru, Yusuke Kato, Kazuki Kozuka, and Aditya Grover. Reflect-dit: Inference-time scaling for text-to-image diffusion transformers via in-context reflection. *arXiv preprint arXiv:2503.12271*, 2025. 2, 3, 5
- [33] Xiner Li, Masatoshi Uehara, Xingyu Su, Gabriele Scalia, Tommaso Biancalani, Aviv Regev, Sergey Levine, and Shuiwang Ji. Dynamic search for inference-time alignment in diffusion models. *arXiv preprint arXiv:2503.02039*, 2025. 2, 3, 5, 8
- [34] Zhiyuan Li, Hong Liu, Denny Zhou, and Tengyu Ma. Chain of thought empowers transformers to solve inherently serial problems. *arXiv preprint arXiv:2402.12875*, 1, 2024. 1, 2
- [35] Zhanhao Liang, Yuhui Yuan, Shuyang Gu, Bohan Chen, Tiankai Hang, Mingxi Cheng, Ji Li, and Liang Zheng. Aesthetic post-training diffusion models from generic preferences with step-by-step preference optimization. In *Proceedings of the Computer Vision and Pattern Recognition Conference*, pages 13199–13208, 2025. 3, 9, 1
- [36] Zhiqiu Lin, Deepak Pathak, Baiqi Li, Jiayao Li, Xide Xia, Graham Neubig, Pengchuan Zhang, and Deva Ramanan. Evaluating text-to-visual generation with image-to-text generation. In *European Conference on Computer Vision*, pages 366–384. Springer, 2024. 3
- [37] Fangfu Liu, Hanyang Wang, Yimo Cai, Kaiyan Zhang, Xiaohang Zhan, and Yueqi Duan. Video-t1: Test-time scaling for video generation. In *International Conference on Computer Vision*, 2025. 3
- [38] Jie Liu, Gongye Liu, Jiajun Liang, Yangguang Li, Jiaheng Liu, Xintao Wang, Pengfei Wan, Di Zhang, and Wanli Ouyang. Flow-grpo: Training flow matching models via online rl. *arXiv preprint arXiv:2505.05470*, 2025. 3
- [39] Zhijian Liu, Ligeng Zhu, Baifeng Shi, Zhuoyang Zhang, Yuming Lou, Shang Yang, Haocheng Xi, Shiyi Cao, Yuxian Gu, Dacheng Li, et al. Nvila: Efficient frontier visual language models. In *Proceedings of the Computer Vision and Pattern Recognition Conference*, pages 4122–4134, 2025. 3
- [40] Nanye Ma, Shangyuan Tong, Haolin Jia, Hexiang Hu, Yu-Chuan Su, Mingda Zhang, Xuan Yang, Yandong Li, Tommi Jaakkola, Xuhui Jia, and Saining Xie. Inference-time scaling for diffusion models beyond scaling denoising steps. In *Proceedings of the IEEE/CVF Conference on Computer Vision and Pattern Recognition (CVPR)*, pages 2523–2534, 2025. 1, 3, 5, 7, 8
- [41] Aman Madaan, Niket Tandon, Prakhar Gupta, Skyler Hallinan, Luyu Gao, Sarah Wiegrefe, Uri Alon, Nouha Dziri, Shrimai Prabhumoye, Yiming Yang, et al. Self-refine: Iterative refinement with self-feedback. *Advances in Neural Information Processing Systems*, 36:46534–46594, 2023. 2
- [42] Niklas Muennighoff, Zitong Yang, Weijia Shi, Xiang Lisa Li, Li Fei-Fei, Hannaneh Hajishirzi, Luke Zettlemoyer, Percy Liang, Emmanuel Candes, and Tatsunori Hashimoto. s1: Simple test-time scaling. In *Workshop on Reasoning and Planning for Large Language Models*. 1, 2
- [43] OpenAI. Learning to Reason with LLMs. OpenAI Project Page, 2023. Accessed: November 2025. 2
- [44] Alexander Pan, Kush Bhatia, and Jacob Steinhardt. The effects of reward misspecification: Mapping and mitigating misaligned models. In *International Conference on Learning Representations*, 2022. 8
- [45] William Peebles and Saining Xie. Scalable diffusion models with transformers. In *Proceedings of the IEEE/CVF international conference on computer vision*, pages 4195–4205, 2023. 1, 2
- [46] Dustin Podell, Zion English, Kyle Lacey, Andreas Blattmann, Tim Dockhorn, Jonas Müller, Joe Penna, and Robin Rombach. Sdxl: Improving latent diffusion models for high-resolution image synthesis. In *The Twelfth International Conference on Learning Representations*. 5, 9, 1
- [47] Yuxiao Qu, Matthew YR Yang, Amrith Setlur, Lewis Tunstall, Edward Emanuel Beeching, Ruslan Salakhutdinov, and Aviral Kumar. Optimizing test-time compute via meta reinforcement finetuning. In *Forty-second International Conference on Machine Learning*. 1
- [48] Alec Radford, Jong Wook Kim, Chris Hallacy, Aditya Ramesh, Gabriel Goh, Sandhini Agarwal, Girish Sastry, Amanda Askell, Pamela Mishkin, Jack Clark, et al. Learning transferable visual models from natural language supervision. In *International conference on machine learning*, pages 8748–8763. PmLR, 2021. 3
- [49] Vignav Ramesh and Morteza Mardani. Test-time scaling of diffusion models via noise trajectory search. *arXiv preprint arXiv:2506.03164*, 2025. 2, 3, 8
- [50] Herbert E Robbins. An empirical bayes approach to statistics. In *Breakthroughs in Statistics: Foundations and basic theory*, pages 388–394. Springer, 1992. 3
- [51] John Schulman, Filip Wolski, Prafulla Dhariwal, Alec Radford, and Oleg Klimov. Proximal policy optimization algorithms. *arXiv preprint arXiv:1707.06347*, 2017. 3
- [52] Jaskirat Singh, Lindsey Li, Weijia Shi, Ranjay Krishna, Yejin Choi, Pang Wei Koh, Michael F Cohen, Stephen Gould, Liang Zheng, and Luke Zettlemoyer. Negative token merging: Image-based adversarial feature guidance. *arXiv preprint arXiv:2412.01339*, 2024. 2, 5, 8, 1, 3
- [53] Raghav Singhal, Zachary Horvitz, Ryan Teehan, Mengye Ren, Zhou Yu, Kathleen McKeown, and Rajesh Ranganath. A general framework for inference-time scaling and steering of diffusion models. In *Forty-second International Conference on Machine Learning*, 2025. 2, 3

- [54] Charlie Snell, Jaehoon Lee, Kelvin Xu, and Aviral Kumar. Scaling llm test-time compute optimally can be more effective than scaling model parameters. *arXiv preprint arXiv:2408.03314*, 2024. 1, 2
- [55] Gemini Team, Rohan Anil, Sebastian Borgeaud, Jean-Baptiste Alayrac, Jiahui Yu, Radu Soricut, Johan Schalkwyk, Andrew M Dai, Anja Hauth, Katie Millican, et al. Gemini: a family of highly capable multimodal models. *arXiv preprint arXiv:2312.11805*, 2023. 1
- [56] Masatoshi Uehara, Yulai Zhao, Chenyu Wang, Xiner Li, Aviv Regev, Sergey Levine, and Tommaso Biancalani. Inference-time alignment in diffusion models with reward-guided generation: Tutorial and review. *arXiv preprint arXiv:2501.09685*, 2025. 1, 3
- [57] Bram Wallace, Meihua Dang, Rafael Rafailov, Linqi Zhou, Aaron Lou, Senthil Purushwalkam, Stefano Ermon, Caiming Xiong, Shafiq Joty, and Nikhil Naik. Diffusion model alignment using direct preference optimization. In *Proceedings of the IEEE/CVF Conference on Computer Vision and Pattern Recognition*, pages 8228–8238, 2024. 3
- [58] Junlin Wang, WANG Jue, Ben Athiwaratkun, Ce Zhang, and James Zou. Mixture-of-agents enhances large language model capabilities. In *The Thirteenth International Conference on Learning Representations*. 1
- [59] Xuezhi Wang, Jason Wei, Dale Schuurmans, Quoc V Le, Ed H Chi, Sharan Narang, Aakanksha Chowdhery, and Denny Zhou. Self-consistency improves chain of thought reasoning in language models. In *The Eleventh International Conference on Learning Representations*, 2023. 1, 2
- [60] Xiyao Wang, Zhengyuan Yang, Linjie Li, Hongjin Lu, Yuancheng Xu, Chung-Ching Lin, Kevin Lin, Furong Huang, and Lijuan Wang. Scaling inference-time search with vision value model for improved visual comprehension. In *Proceedings of the IEEE/CVF International Conference on Computer Vision*, pages 1173–1184, 2025. 3
- [61] Yibin Wang, Yuhang Zang, Hao Li, Cheng Jin, and Jiaqi Wang. Unified reward model for multimodal understanding and generation. *arXiv preprint arXiv:2503.05236*, 2025. 3
- [62] Jason Wei, Xuezhi Wang, Dale Schuurmans, Maarten Bosma, Fei Xia, Ed Chi, Quoc V Le, Denny Zhou, et al. Chain-of-thought prompting elicits reasoning in large language models. *Advances in neural information processing systems*, 35:24824–24837, 2022. 1, 2
- [63] Thaddäus Wiedemer, Yuxuan Li, Paul Vicol, Shixiang Shane Gu, Nick Matarese, Kevin Swersky, Been Kim, Priyank Jaini, and Robert Geirhos. Video models are zero-shot learners and reasoners. *arXiv preprint arXiv:2509.20328*, 2025. 1
- [64] Chenfei Wu, Jiahao Li, Jingren Zhou, Junyang Lin, Kaiyuan Gao, Kun Yan, Sheng-ming Yin, Shuai Bai, Xiao Xu, Yilei Chen, et al. Qwen-image technical report. *arXiv preprint arXiv:2508.02324*, 2025. 1
- [65] Xiaoshi Wu, Yiming Hao, Keqiang Sun, Yixiong Chen, Feng Zhu, Rui Zhao, and Hongsheng Li. Human preference score v2: A solid benchmark for evaluating human preferences of text-to-image synthesis. *arXiv preprint arXiv:2306.09341*, 2023. 3, 5
- [66] Xun Wu, Shaohan Huang, and Furu Wei. Multimodal large language model is a human-aligned annotator for text-to-image generation. *arXiv preprint arXiv:2404.15100*, 2024. 3
- [67] Enze Xie, Junsong Chen, Yuyang Zhao, Jincheng YU, Ligeng Zhu, Yujun Lin, Zhekai Zhang, Muyang Li, Junyu Chen, Han Cai, et al. Sana 1.5: Efficient scaling of training-time and inference-time compute in linear diffusion transformer. In *International Conference on Machine Learning*, 2025. 1, 3
- [68] Xin Xie and Dong Gong. Dymo: Training-free diffusion model alignment with dynamic multi-objective scheduling. In *Proceedings of the Computer Vision and Pattern Recognition Conference*, pages 13220–13230, 2025. 3
- [69] Jiazheng Xu, Xiao Liu, Yuchen Wu, Yuxuan Tong, Qinkai Li, Ming Ding, Jie Tang, and Yuxiao Dong. Imagereward: Learning and evaluating human preferences for text-to-image generation. In *NeurIPS*, pages 15903–15935, 2023. 3, 5
- [70] Jiazheng Xu, Yu Huang, Jiale Cheng, Yuanming Yang, Jiajun Xu, Yuan Wang, Wenbo Duan, Shen Yang, Qunlin Jin, Shurun Li, et al. Visionreward: Fine-grained multi-dimensional human preference learning for image and video generation. *arXiv preprint arXiv:2412.21059*, 2024. 3
- [71] Zeyue Xue, Jie Wu, Yu Gao, Fangyuan Kong, Lingting Zhu, Mengzhao Chen, Zhiheng Liu, Wei Liu, Qiushan Guo, Weilin Huang, et al. Dancegrpo: Unleashing grpo on visual generation. *arXiv preprint arXiv:2505.07818*, 2025. 3
- [72] Kai Yang, Jian Tao, Jiafei Lyu, Chunjiang Ge, Jiaxin Chen, Weihan Shen, Xiaolong Zhu, and Xiu Li. Using human feedback to fine-tune diffusion models without any reward model. In *Proceedings of the IEEE/CVF Conference on Computer Vision and Pattern Recognition*, pages 8941–8951, 2024. 3
- [73] Qiyuan Zhang, Fuyuan Lyu, Zexu Sun, Lei Wang, Weixu Zhang, Wenyue Hua, Haolun Wu, Zhihan Guo, Yufei Wang, Niklas Muennighoff, Irwin King, Xue Liu, and Chen Ma. A survey on test-time scaling in large language models: What, how, where, and how well?, 2025. 2
- [74] Tao Zhang, Cheng Da, Kun Ding, Huan Yang, Kun Jin, Yan Li, Tingting Gao, Di Zhang, Shiming Xiang, and Chunhong Pan. Diffusion model as a noise-aware latent reward model for step-level preference optimization. *arXiv preprint arXiv:2502.01051*, 2025. 3
- [75] Yinan Zhang, Eric Tzeng, Yilun Du, and Dmitry Kislyuk. Large-scale reinforcement learning for diffusion models. In *European Conference on Computer Vision*, pages 1–17. Springer, 2024. 3
- [76] Denny Zhou, Nathanael Schärli, Le Hou, Jason Wei, Nathan Scales, Xuezhi Wang, Dale Schuurmans, Claire Cui, Olivier Bousquet, Quoc V Le, and Ed H. Chi. Least-to-most prompting enables complex reasoning in large language models. In *The Eleventh International Conference on Learning Representations*, 2023. 2
- [77] Zikai Zhou, Shitong Shao, Lichen Bai, Shufei Zhang, Zhiqiang Xu, Bo Han, and Zeke Xie. Golden noise for diffusion models: A learning framework. In *Proceedings*

of the IEEE/CVF International Conference on Computer Vision, pages 17688–17697, 2025. [3](#), [9](#)

- [78] Zikai Zhou, Shitong Shao, Lichen Bai, Shufei Zhang, Zhiqiang Xu, Bo Han, and Zeke Xie. Golden noise for diffusion models: A learning framework. In *International Conference on Computer Vision*, 2025. [2](#)
- [79] Le Zhuo, Liangbing Zhao, Sayak Paul, Yue Liao, Renrui Zhang, Yi Xin, Peng Gao, Mohamed Elhoseiny, and Hongsheng Li. From reflection to perfection: Scaling inference-time optimization for text-to-image diffusion models via reflection tuning. In *Proceedings of the IEEE/CVF International Conference on Computer Vision*, pages 15329–15339, 2025. [3](#)

TTSnap: Test-Time Scaling of Diffusion Models via Noise-Aware Pruning

Supplementary Material

A. SDXL Experiments

In this section, we outline several experiments making use of the SDXL [46] model, allowing compatibility assessment and fair comparison with approaches trained on this model.

A.1. TTSnap Performance on SDXL

Like the experiments on FLUX [3], we evaluate TTSnap on SDXL [46] under both the single-reward and multi-reward scenarios. We first finetune all the reward models to be noise-aware using 5,000 training prompts with 8 images generated per prompt, following the same learning rate, scheduler, and training-epoch configurations as in Sec. 6.1 We then assess test-time search performance on a separate validation set of 200 prompts. For NegToMe [52], we set the merging alpha to 2.5 and the merging threshold to 0.7 in both the training and validation sets. After searching for the optimal pruning configuration, we use $\mathcal{T} = \{6, 9, 13\}$ and $\mathcal{A} = \{0.6, 0.6, 0.7\}$ when pruning with our finetuned noise-aware reward models. For early-step pruning without noise-aware finetuning, the best-performing configuration is $\mathcal{T} = \{9, 14\}$ and $\mathcal{A} = \{0.6, 0.7\}$. The corresponding results are reported in Tab. 4 under a computation budget range from 200 TFlops to 4000 TFlops.

As shown in Tab. 4, TTSnap also improves test-time search performance on SDXL under a range of computation budgets. However, the gains are less pronounced compared to Flux. We attribute this gap to three main factors. First, the Kendall correlation of SDXL’s noise-aware reward models is consistently lower than that of Flux—approximately 0.15 lower on average at each timestep. A weaker base model yields a lower quality of posterior mean (Tweedie) estimates, which in turn weakens the noise-aware reward outcomes. This also explains why the optimal pruning steps \mathcal{T} for SDXL needs to be set to higher timesteps (closer to clean images) compared to Flux. Second, SDXL incurs a higher VAE decoding cost relative to its denoising steps, making verification more expensive. Under the same test-time search budget, this limits the number of candidate trajectories that can be explored compared to Flux. Third, Flux has stronger generative ability and covers a wider range of distributions, resulting in higher diversity for the same prompt. To quantify this effect, we compute the standard deviation of reward scores. For Flux, the standard deviations for ImageReward, PickScore, and HPS are 0.474, 6.14e-3, and 8.21e-3, respectively, whereas SDXL shows lower diversities of 0.4586, 5.74e-3, and 7.2e-3.

Table 4. Evaluation of TTSnap performance on SDXL. As for Flux, we compare the best-of- N (BoN) strategy, pruning without NARF (TTSp), and pruning with NARF (TTSnap) under single-reward and combined-reward settings. The top row indicates the reward model used by the algorithm and the second row indicates the reward model used for evaluation. We report the final reward values for compute budgets $B = 1k, 2k, 4k$ TFLOPs, along with the relative gain ω over best-of- N . $r(B \rightarrow 0)$ denotes the expected reward of sampling one image per prompt at random.

	Alg. Reward:	IR	Pick	HPS	All	All	All
	Eval. Reward:	IR	Pick	HPS	IR	Pick	HPS
–	$r(B \rightarrow 0)$	0.821	.2086	.2798	0.819	.2085	.2797
BoN	$r(B = 1k)$	1.354	.2162	.2898	1.219	.2143	.2871
	$r(B = 2k)$	1.435	.2178	.2921	1.282	.2154	.2886
	$r(B = 4k)$	1.490	.2189	.2938	1.327	.2162	.2897
TTSp	$r(B = 1k)$	1.370	.2164	.2898	1.232	.2144	.2872
	$r(B = 2k)$	1.450	.2179	.2921	1.297	.2155	.2887
	$r(B = 4k)$	1.503	.2189	.2939	1.340	.2163	.2898
	ω (%)	3.0	4.24	0.19	4.15	1.67	2.42
TTSnap	$r(B = 1k)$	1.396	.2170	.2903	1.254	.2150	.2877
	$r(B = 2k)$	1.470	.2184	.2925	1.306	.2160	.2891
	$r(B = 4k)$	1.515	.2194	.2941	1.348	.2167	.2901
	ω (%)	5.75	7.16	2.42	6.85	9.52	5.99

A.2. Noise-aware Reward Model Comparison

SPO [35] also trains a PickScore-based noise-aware reward model, termed SPM (Step Preference Model), using SDXL samples for diffusion model finetuning. Compared to ours, the primary limitation of SPM is its lack of efficiency. The method uses human-labeled preference pairs, forwards the same noise to both samples, and trains the model with a Bradley–Terry loss [7]. They use AdaLN [45] to enable time-conditioned generation. However, the forward diffusion trajectories follow conditional distributions induced by the provided data, while inference-time trajectories are sampled from the marginal distribution. Only with extensive training on a large dataset, conditional diffusion trajectories can approximate the marginal distribution, but this requires a high cost, e.g., SPM is trained for 29 hours on half a million images. In contrast, since our goal is TTS, we train the reward model directly on diffusion trajectories sampled from diverse random noise, producing a reward model that is naturally aligned with the distributions encountered during inference. We use their pretrained SPM checkpoints for SDXL and compare the Kendall coefficient against their method for all the inference steps in Fig. 8. Their perfor-

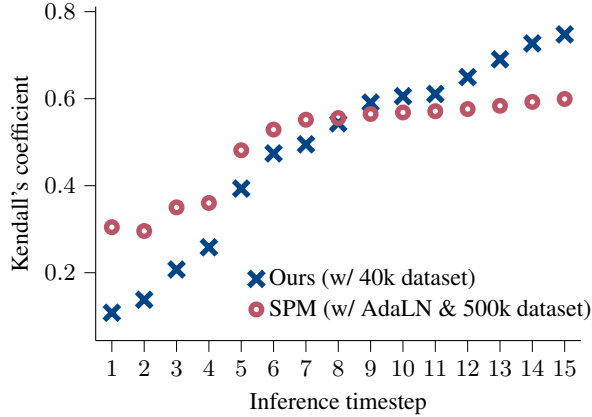


Figure 8. Compare our finetuned noise-aware reward and SPM for PickScore on SDXL.

mance drops at higher timesteps due to uniform timestep sampling during training, which leads to loss imbalance. Further analysis of this issue is provided in Sec. B.2. We underperform their method at lower timesteps, but their training data volume is substantially larger than ours. Our performance improves steadily with increased data size, as demonstrated in Sec. B.1.

B. Further NARF Analyses

In this section, we report further analyses on our noise-aware reward model and compare it to other variants.

B.1. Effect of Data Scaling

Our self-distillation pipeline does not rely on human-annotated data, enabling us to generate training sets of arbitrary size. Following the setup in our main experiments, we sample 8 images per prompt and progressively double the number of prompts up to 5,000. As shown in Fig. 9, increasing the dataset size by multiples leads to consistent, approximately linear improvements in Kendall’s correlation across timesteps. This trend highlights the strong potential of our noise-aware reward model to further improve with additional data scaling.

B.2. Curriculum Learning Strategy Analysis

Instead of our proposed curriculum approach, which trains noise-aware reward models from higher timesteps to lower, noisier ones, we consider two alternative training strategies for NARF. The first separately finetunes each timestep by initializing from the original model weights. The second trains a single time-conditioned reward model by uniformly sampling timesteps at each iteration. We compare both alternatives on ImageReward under the same total number of training epochs, evaluating using Kendall’s τ coefficient in Tab. 5. For the first alternative, we find that it consistently

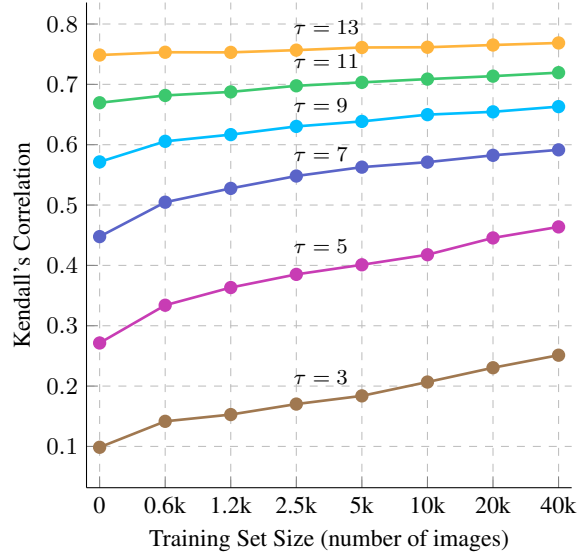


Figure 9. The effect of scaling the training data for different noise timesteps τ . Kendall’s correlation increases approximately linearly with each doubling of the training set size. Note that the x-axis is shown on a logarithmic scale.

underperforms our curriculum strategy, especially at lower timesteps, where the domain gap becomes larger.

To evaluate the second alternative, we adopt the design of DiT [45] to integrate timestep embeddings as conditional input, by adding adaptive layer-norm (AdaLN) blocks to the ImageReward ViT backbone. Although this approach and our curriculum strategy achieve similar overall performance, the time-conditioned model incurs a significant model size increase (445M \rightarrow 601M). To ensure a fair comparison, we also evaluate our curriculum strategy using the same AdaLN-augmented model architecture. Under equal model capacity, the curriculum method leads to higher Kendall correlation across timesteps, especially at those closer to the clean image.

These result reveal two key limitations of uniform-timestep training. First, the model performs slightly worse at larger timesteps due to loss imbalance: early noisy samples dominate the training because their losses are much larger, while later cleaner samples contribute very little. Although loss reweighting may mitigate this issue, it can slow down training because higher weights must be assigned to the easy (later) timesteps, and selecting a proper weighting scheme is non-trivial. Second, the model architecture has to be scaled up to include timestep-conditioning blocks, which increases both training and test-time verification cost. In contrast, the curriculum strategy is simpler and easier to implement: it requires no architectural changes and treats the reward model as a black box, making it a more general way to adopt across different models. Therefore, we choose

to use the original reward model architecture together with the curriculum strategy for NARF.

B.3. Loss Function Analysis

Reward models on clean images are typically trained with a rank-forcing loss on paired data with annotated human preferences, since obtaining ground-truth absolute scores for arbitrary images is often impractical. However, in our distillation setting, the ground-truth reward values are fully available, allowing us to form the training as a regression task rather than a pure ranking-based one. We compare these two training paradigms when finetuning our noise-aware reward model. Under the ranking formulation, we randomly sample two images from the same prompt and apply the Bradley–Terry loss [7]

$$\mathcal{L}_{BT} = -\frac{\exp(\lambda \cdot r^+)}{\exp(\lambda \cdot r^+) + \exp(\lambda \cdot r^-)} \quad (12)$$

where $\lambda \in \mathbb{R}$ is the temperature, r^+ and r^- denote the predicted rewards of the higher and lower ranked samples. This objective imposes a strong penalty whenever the model’s predicted ordering deviates from the ground-truth ranking. Under the regression formulation, we simply optimize a standard MSE loss. Empirically, as shown in Tab. 6, we find the MSE loss outperforms the Bradley–Terry loss. A plausible explanation is that MSE provides a dense and informative supervisory signal by supervising absolute reward magnitudes, whereas Bradley–Terry ignores absolute values and supervises only pairwise order.

C. Limitations and Future Work

Noise-aware Rewards in Latent Space. We finetune existing image-based reward models to be noise-aware, enabling early-stage pruning for test-time scaling. Since the majority of large-scale pretrained diffusion models are latent diffusion models, validating candidates with our noise-aware reward models requires computing the posterior mean, decoding it through the VAE, and then scoring the resulting image. As shown in the TFLOPs breakdown Tab. 7, VAE decoding is the dominant component of the verification cost. Consequently, a high verification budget reduces the effective search capacity of TTSnap under a fixed total budget, limiting exploration. A promising direction for future work is to develop a noise-aware reward model that operates directly in the latent space [20, 74], thereby avoiding the expensive VAE decoding. This would require a different model architecture and training strategy, as our current self-distillation strategy, which finetunes the reward model on the pixel domain, would no longer be applicable.

Adapt Different Types of Reward Models. The reward models used in our paper [28, 65, 69] are based on BLIP [31] or CLIP [48]. They primarily assess overall

semantic and aesthetic quality. There are also alternative types of reward models. For example, some are based on vision–language models, which can evaluate specific given attributes [36, 39, 61, 70], while some are based on detection backbones to assess object counts or compositional structure [5, 19]. Although some of these models may be too heavy for test-time scaling [61, 70], they could still be incorporated into a multi-stage search pipeline once the candidate pool has been narrowed down. Given that these reward models differ substantially in architecture, the procedure for finetuning them to be noise-aware may also vary accordingly. It would be beneficial to apply our method to a broader range of reward models.

D. Further Details

Further Evaluation Details. The metric ω as defined in Sec. 4 measures the difference between two integrated improvements of the reward over the budget range $[B^-, B^+]$. If $\omega > 0$, the algorithm performs better than the reference one, and vice versa. The integration is computed using Simpson’s rule. For both Flux and SDXL, we set B^- and B^+ to span the interval from 200 to 4000 TFLOPs. Here, we choose B^- to be the budget at which the search is limited to a single candidate, ensuring that both curves start from the same initial point. To compute the number of candidates under a given budget, the TFLOPs of each component are referenced in Tab. 7.

To evaluate the rank consistency of our noise-aware reward models with respect to the final denoised images, we adopt Kendall’s rank correlation coefficient [24]. Given two rankings over the same set of items, the coefficient is defined as

$$\mathcal{K} = \frac{C - D}{\binom{n}{2}} = 1 - \frac{2D}{\binom{n}{2}}, \quad (13)$$

where C and D denote the numbers of concordant and discordant pairs, respectively. A pair (i, j) is concordant if the two rankings agree on their relative order and discordant otherwise. The number of discordant pairs corresponds to the number of swaps that bubble sort would perform to transform one ranking into the other. Since Kendall’s τ depends solely on the ordering rather than the magnitude of the rank values, it penalizes only ordinal inconsistencies. Identical rankings receive a score of 1, completely reversed rankings receive -1 , and independent random rankings have an expected value of 0.

Further Implementation Details. All HPS scores reported in this paper refer to HPSv2. All validation sets and training sets images used in the experiments are generated with NegToMe [52] using the same hyperparameter configurations. We follow the original NegToMe parameter settings, with a slight increase in the merging alpha to promote

Table 5. We compare several noise-aware training strategies across all inference timesteps under the same total number of training epochs, including: (i) separately training each timestep initialized from the pretrained reward model (Sep); (ii) our curriculum strategy that trains from higher timesteps and gradually shifts to lower ones (Cur); (iii) uniformly sampling timesteps and training a time-conditioned model by adding AdaLN (Uni w/ AdaLN); and (iv) the same AdaLN-augmented model trained with the curriculum strategy to ensure a fair comparison under equal model capacity with the previous one.

method	Kendall’s coefficient of each inference timestep														
	1	2	3	4	5	6	7	8	9	10	11	12	13	14	15
Baseline	.008	.020	.099	.168	.271	.370	.448	.513	.572	.622	.670	.709	.749	.782	<u>.811</u>
Sep (445M)	.050	.085	.199	.285	.427	.517	.570	.615	.651	.680	.713	<u>.742</u>	<u>.769</u>	.791	.810
Cur (445M)	.062	.130	.251	<u>.330</u>	.464	<u>.544</u>	<u>.592</u>	.629	<u>.663</u>	<u>.689</u>	<u>.719</u>	<u>.742</u>	<u>.769</u>	<u>.792</u>	.810
Uni (w/ AdaLN- t , 601M)	.053	<u>.132</u>	<u>.253</u>	.338	<u>.466</u>	.541	.591	<u>.631</u>	<u>.663</u>	<u>.689</u>	.712	.733	.751	.765	.777
Cur (w/ AdaLN, 601M)	<u>.056</u>	.134	.250	.329	.469	.549	.602	.643	.679	.708	.736	.760	.788	.813	.833

Table 6. Comparison of MSE loss and Bradley–Terry loss on finetuning noise-aware ImageReward.

Loss option	Kendall’s coefficient of each inference timestep														
	1	2	3	4	5	6	7	8	9	10	11	12	13	14	15
Bradley–Terry	0.074	0.144	0.261	0.332	0.450	0.529	0.577	.610	0.637	0.659	0.682	0.709	.730	0.754	0.779
MSE	0.062	0.130	0.251	0.330	0.464	0.544	0.592	0.629	0.663	0.689	0.719	0.742	0.769	0.792	.810

Table 7. We report the TFLOPs for a single functional call of each model used in this paper. For the SDXL diffusion model, we list the TFLOPs of two functional calls for classifier-free guidance.

Model	TFLOPs
Flux VAE decoder	1.243
Flux diffusion model	9.927
SDXL VAE decoder	4.970
SDXL diffusion model ($\times 2$)	5.982
ImageReward model	0.068
PickScore model	0.185
HPS model	0.185

higher diversity. Setting the merging alpha too high would degrade text–image alignment. We use a linear learning-rate scheduler when training the noise-aware reward models, and the learning rate is linearly decayed to 0.5 of its initial value. We set the inference steps for both Flux and SDXL to 20. When training the noise-aware reward models, we begin only from step 15 for two reasons. First, for very late timesteps (close to the final image), noise-aware rewards have marginal improvement after training. Second, including these steps provides little benefit during test-time search, as they save very little computation and thus contribute minimally to exploration under a fixed budget.